Conical Diffraction and Composite Lieb Bosons in Photonic Lattices

Falko Diebel,[1,*] Daniel Leykam,[2,3] Sebastian Kroesen,[1] Cornelia Denz,[1] and Anton S. Desyatnikov[2,4]
[1]Institut für Angewandte Physik and Center for Nonlinear Science (CeNoS), Westfälische Wilhelms-Universität Münster, 48149 Münster, Germany
[2]Nonlinear Physics Centre, Research School of Physics and Engineering, The Australian National University, Canberra, Australian Capital Territory 0200, Australia
[3]Division of Physics and Applied Physics, School of Physical and Mathematical Sciences, Nanyang Technological University, Singapore 637371, Singapore
[4]Department of Physics, Nazarbayev University, 53 Kabanbay Batyr Avenue, Astana 010000, Kazakhstan
(Received 13 October 2015; revised manuscript received 4 March 2016; published 4 May 2016)

Pseudospin describes how waves are distributed between different "internal" degrees of freedom or microscopic states, such as polarizations, sublattices, or layers. Here, we experimentally demonstrate and explain wave dynamics in a photonic Lieb lattice, which hosts an integer pseudospin $s = 1$ conical intersection. We study the most striking differences displayed by integer pseudospin states: pseudospin-dependent conical diffraction and the generation of higher charged optical vortices.

DOI: 10.1103/PhysRevLett.116.183902

Dirac cones in the energy spectrum of graphene appear due to its two inequivalent sublattices: these two degrees of freedom of an electron wave result in a half-integer spin analogue, the "pseudospin" $m_s = \pm 1/2$, reflecting the fermionic nature of low-energy quasiparticles [1]. In photonics, powerful analogies between pseudospin and "real" spin intuitively explain complicated effects such as perfect nonresonant Klein tunneling [2,3], photon absorption in graphene [4], and optical vortex generation during conical diffraction [5,6].

Specially designed lattices can overcome the fermion limit as, for example, in photonic graphene [7–10] and reveal states with higher pseudospin, e.g., the Lieb lattice [11–18] with three intersecting energy bands and an integer pseudospin triplet, $m_s = 0, \pm 1$ [19–22]. Corresponding quasiparticles raise a number of intriguing questions. What are the differences between Dirac fermions and composite Lieb bosons with integer pseudospin? Are there analogies between wave packets with pseudospin-one and spin-one photons? How can we harness unique effects associated with higher pseudospin states in future photonic devices?

Integer pseudospin intersections fundamentally differ from the more familiar Dirac cones. They necessarily involve a dispersionless flat band with infinite effective mass hosting compact localized states useful for realizing strongly interacting phases of light and matter [16–18]. The near degeneracy of other bands with zero effective mass is ideal for switching applications and enables novel topological phases with protected edge states in resonance with flat band states [13,23,24]. A vanishing Berry phase around integer pseudospin intersections suppresses weak antilocalization effects found at $s = 1/2$ Dirac cones [25,26]. These interesting features associated with integer pseudospin were not observed in experiments yet: unlike Dirac cones, higher-order intersections are not protected, and perturbations can either open a gap or split them into pairs of Dirac cones [27], thus revealing the composite nature of corresponding quasiparticles [28].

We realize the higher-order band intersection in a photonic Lieb lattice and directly probe its pseudospin $m_s = 0, \pm 1$ states using structured light. Additionally, we establish the special role played by eigenstates of the pseudospin operator $\hat{S}_z$ with eigenvalues m_s: their propagation yields a generalized, pseudospin-dependent conical diffraction. The transitions between different $\hat{S}_z$ eigenstates produce a series of phase vortices with charges $l = m_{s,f} - m_{s,i}$, where $m_{s,f}$ and $m_{s,i}$ label the final and initial eigenstates, generalizing the vortex generation recently observed in photonic graphene [6]. This vortex generation is a consequence of the *nontrivial winding* of the Bloch modes around the conical intersection, but it is not a simple Berry phase effect. Our pseudospin formalism unifies the description of the fermionic and bosonic conical intersections, and it applies to other wave systems beyond photonics, such as electrons in condensed matter, as well as cold atoms and matter waves in optical lattices.

We fabricated the photonic Lieb lattice in fused silica glass using direct femtosecond laser writing [29] [Fig. 1(a)]. The lattice contains 15×15 unit cells with three sublattices labeled as A, B, C. The lattice period is $a = 30\,\mu$m (neighboring waveguide separation $15\,\mu$m), with a propagation length of $L = 30\,$mm. The inscription setup is based on a Ti:sapphire femtosecond laser system with pulse energies up to 1 mJ at 1 kHz repetition rate. The laser pulses are attenuated and focused using a 50× ultralong working distance microscope objective with a numerical aperture of NA = 0.55. To obtain high contrast and ideal coupling between the permanent waveguides, the pulse energy was set to 85 nJ with a sample translation velocity of $150\,\mu\text{ms}^{-1}$. Because of the large extent of the

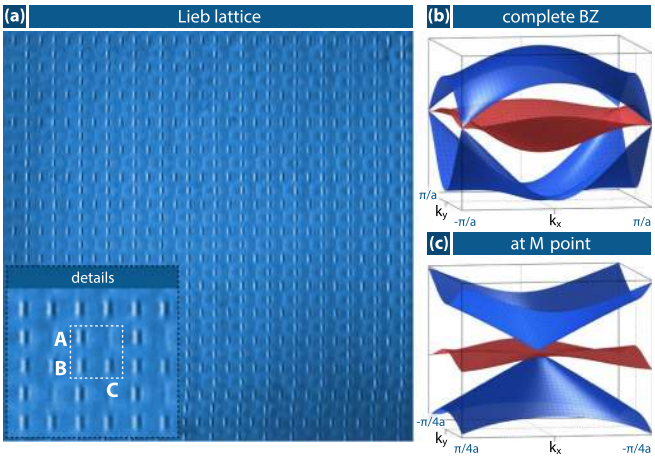

FIG. 1. Two-dimensional photonic Lieb lattice in fused silica. (a) Phase contrast image of the fabricated refractive index profile $n(x, y)$. The inset shows a magnification of few unit cells with the three sublattices labeled as A, B, C. (b),(c) Numerical simulations of the lattice band structure showing the whole Brillouin zone and the area around the M point, respectively. The conical intersection at the Brillouin zone corner (M point) and the additional quasi-flat-band in the middle is cleary visible.

inscribed lattices, the pulse energy is automatically adapted to the addressed inscription depth to compensate for absorption and spherical aberrations.

To directly probe conical dispersion, we require a broad, structured excitation of the three sublattices, in contrast to previous experiments considering the propagation of narrow, localized wave packets [15–17]. Therefore, we employ high-resolution phase-only spatial light modulators to have full control over the probe beam's amplitude and phase profile. The broad $\hat{S}_z$ eigenstates then generate different conical diffraction patterns during propagation [21]. Illuminating only the B sublattice excites the $m_s = 0$ eigenstate, for which the resulting output shown in Figs. 2(a) and 2(b) strongly depends on both the full width at half maximum w of its Gaussian envelope and the beam tilt. In contrast, a narrow wave packet with $w \sim a$ excites the whole Brillouin zone, thus generating a discrete diffraction pattern with pronounced square symmetry [15], as can be seen in the second column of Fig. 2. Increasing the envelope width w and approaching the continuum limit $w \gg a$, there is a transition to regular diffraction at the Γ point (flat phase profile), while at the M point (staggered phase) we observe conical diffraction with rapidly expanding rings (right-hand columns of Fig. 2).

A distinguishing feature of our higher-order intersection is the existence of three different pseudospin eigenstates, $m_s = 0, \pm 1$. This is in contrast to spin-one photons, which are transverse waves with only two distinct spin states permitted, namely, left- and right-handed circular polarizations. The two pseudospin eigenstates with $|m_s| = 1$, analogous to circular polarization states of light, excite the A and C sublattices and host a series of phase vortices. While their output conical diffraction intensity profiles, e.g. $m_s = -1$ in Fig. 2c still have an expanding ring of higher

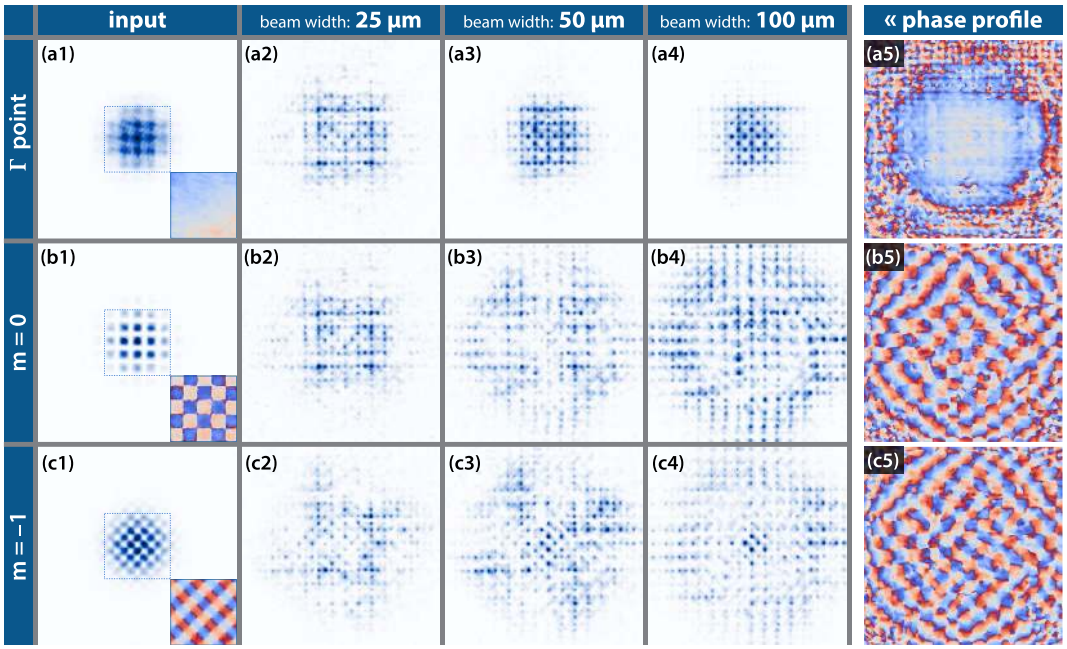

FIG. 2. Transition from discrete to conical diffraction. Intensity and phase profiles during the transition from discrete to conical diffraction as the input wave packet width w is increased. (a) Conventional diffraction at Γ point, (b) conical diffraction of $m_s = 0$ pseudospin eigenstate at M point, and (c) pseudospin $m_s = -1$ eigenstate at M point. Left-hand column: Intensity and phase (inset) distribution at the input. Right-hand column: Phase profiles at the output. All panels are normalized individually.

intensity, there is also a bright central spot, due to additional excitation of the middle "flat" band [21].

We quantify the transition from regular to conical diffraction by plotting the growth of the second moment $\Delta\mu_2 = \mu_2(L) - \mu_2(0)$ depending on the envelope width w (see Fig. 3). Here, $\mu_2(z) = \int dxdy[(x-\bar{x})^2 + (y-\bar{y})^2]|\times E(x,y,z)|^2$, where $(\bar{x},\bar{y})$ is the beam's center of mass (see Supplemental Material [30]). The change of the second moment $\Delta\mu_2$ is sensitive to the wave packet's mean squared group velocity $\langle v_G^2\rangle$. At the Γ point (parabolic dispersion), where $\langle v_G^2\rangle \to 0$ for $w \gg a$, a broad Gaussian beam expands more slowly. On the other hand, conical intersections display an *anomalous* scaling, with $\langle v_G^2\rangle$ approaching a maximum for increasing beam width w. For a pseudospin-one eigenstate the mean squared group velocity depends on the initial pseudospin eigenvalue m_s (see Supplemental Material [30]). Thus, at higher pseudospin intersections, the expansion rate for wave packets with larger $|m_s|$ expands more slowly, as observed in Fig. 3. This represents a generalization of the more familiar $s = 1/2$ conical diffraction in biaxial crystals [5] and honeycomb lattices [7], where the mean squared group velocity can have only one value.

If we look at the phase profiles generated by the conical diffraction of the pseudospin eigenstates, they contain a structured pattern of optical vortices (Fig. 2, right-hand column). We now highlight the role of s and m_s on the phase profiles. Around the conical intersection, the propagating modes acquire a Berry phase: π for half-integer s and 0 (mod 2π) for integer s. Despite this trivial phase winding, the modes at integer s intersections still display *another* type of nontrivial "winding," which we can measure using the output phase profiles.

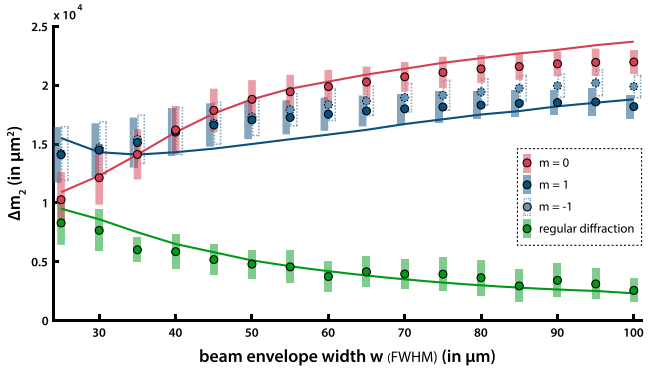

FIG. 3. Wave packet spreading $\Delta\mu_2$ for the different pseudospin states as input beam width w is increased. For regular diffraction at Γ point (green) the spreading $\Delta\mu_2$ decreases. In contrast, for $m_s = 0, \pm 1$ wave packet spreading increases to maximum at conical intersection [green, $m_s = 0$; blue, $m_s = -1$ (coincides within error bars)]. Circles and error bars, from experiments; curves, simulations. Because of the finite beam size, the effect is not as strong as predicted by theory of infinitely extended waves. (See Supplemental Material [30].)

Projecting the output field onto the different pseudospin eigenstates, we expect the phase profile to simplify noticeably. If we consider the evaluation of a pseudospin eigenstate $|m_{s,i}\rangle$ and project the resulting output field onto the different pseudospin eigenstates $|m_{s,f}\rangle$, this reveals a single vortex with charge $l = m_{s,f} - m_{s,i}$ in each component $|m_{s,f}\rangle$.

The projection of the output field on the pseudospin eigenstates is relatively simple for the $s = 1/2$ honeycomb lattice because $\hat{S}_z$ is diagonal in the natural sublattice basis. Thus, measuring the output on a single sublattice will remove the unwanted pseudospin eigenstate. In contrast, in the Lieb lattice $\hat{S}_z$ is *not* diagonal in this basis—its eigenstates involve superpositions of different sublattices, $|0\rangle = \psi_B$ and $|\pm 1\rangle = (\psi_A \pm i\psi_C)/\sqrt{2}$ (see Supplemental Material [30]). In principle, one could terminate the array with appropriately designed coherent couplers between the A and C sublattices to obtain the required superpositions. Here, we instead directly measure the output intensity and phase at each waveguide, and then postprocess the data to filter out the unwanted pseudospin eigenstates (see Supplemental Material [30]).

These vortices are an *additional* consequence of the nontrivial winding of the modes at the conical intersection, and they exist for all s, even integer values when the Berry phase vanishes. This effect can be seen nicely by introducing raising and lowering operators to express the pseudospin operator and recasting the Bloch Hamiltonian in the polar coordinate system $\mathbf{p} = (p_x, p_y, p_z) = (p\cos\vartheta, p\sin\vartheta, 0)$ as (see Supplemental Material [30])

$$\hat{H}(\mathbf{p}) \propto [e^{-i\vartheta}\hat{S}_+ + e^{i\vartheta}\hat{S}_-]. \tag{1}$$

Consequently, the propagation raises (lowers) the pseudospin S_z while introducing an $e^{-i\vartheta}$ ($e^{i\vartheta}$) phase factor, which creates a negative (positive) phase winding, or optical vortex. Intuitively, this vortex generation enforces conservation of the total angular momentum $\hat{J}_z = \hat{S}_z + \hat{L}_z$, which is required by the rotational symmetry of the Bloch Hamiltonian [4,21].

The simulated output pseudospin components (intensity and phase) as a function of the input pseudospin eigenstate are shown in Fig. 4. There are two special features that are unique to integer pseudospin intersections, and do not occur at a half-integer Dirac cone: the generation of double charge vortices when $m_{s,i} = \pm 1$ is converted to $m_{s,f} = \mp 1$ [cf. Fig. 4 (top right and bottom left)] and the existence of a time reversal invariant $m_s = 0$ eigenstate, for which the sum of the output vortex charges vanishes [cf. Fig. 4 (middle)]. Notice how in some cases there are additional vortex-antivortex pairs—a consequence of the finite beam size.

Figure 5 shows the corresponding experimental observations, which demonstrate good overall agreement with both the simulations and the vortex charge rule. Some small

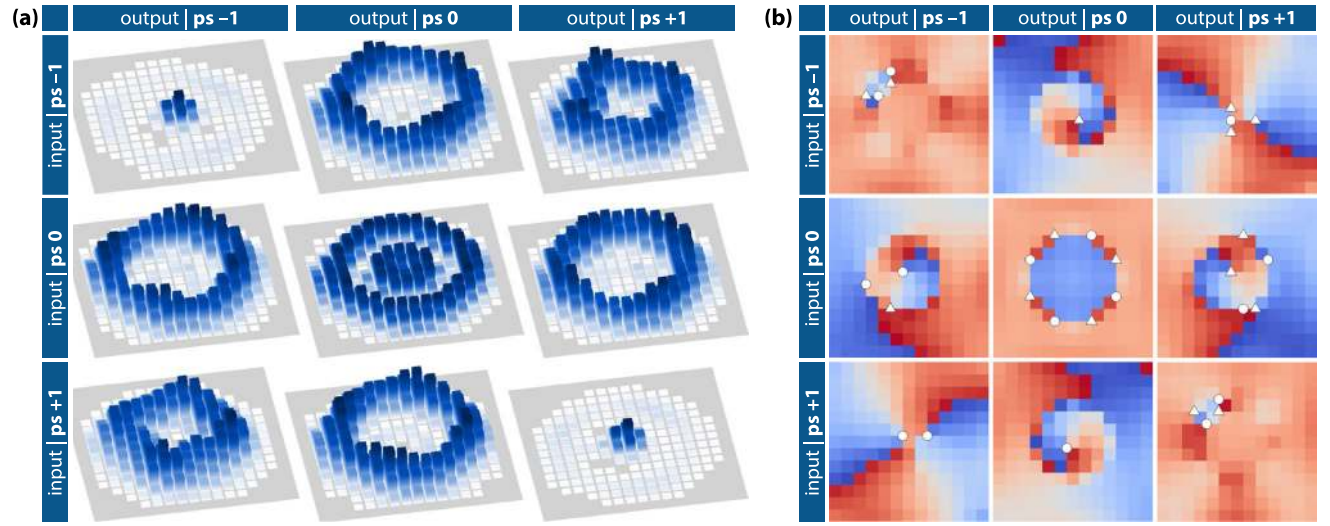

FIG. 4. Numerically obtained pseudospin-mediated optical vortex generation. (a) Intensity and (b) phase distribution of the different output pseudospin components as a function of the input eigenstate. White circles (triangles) mark positions of negative (positive) vortices. The total vortex charge $l = m_{s,f} - m_{s,i}$ conserves $J_z = L_z + S_z$. Each pixel in these images represents the intensity or phase in one unit cell according to the particular pseudospin polarizing filter (see Supplemental Material [30]).

asymmetry and experimental noise produce additional vortex-antivortex pairs while preserving the total charge. The finite size of our lattice results in an obvious discreteness in the output profiles. Although there is only rotational symmetry in the continuum limit, the charge rule remains robust, most prominently the generation of double charge vortices. This observed behavior is in close analogy to the generation of optical vortices via spin-orbit interaction of light [31], with pseudospin replacing spin and projection corresponding to a circular polarizing filter. However, while light is decomposed into two states (left- and right-handed circular polarizations), here there are $2s + 1$ distinct pseudospin states and the form of the pseudospin filter depends on the lattice geometry (see Supplemental Material [30]).

In conclusion, we have generated integer pseudospin states and directly observed their conical diffraction at higher-order, $s = 1$, conical intersection in a photonic Lieb lattice. This generalizes the interesting properties of $s = 1/2$ Dirac cones in graphene and its photonic analogues to integer pseudospin, thus opening up a "third dimension" to the spin of light. We observed two distinguishing features of higher-order conical intersections: pseudospin-dependent conical diffraction, with higher pseudospin eigenstates

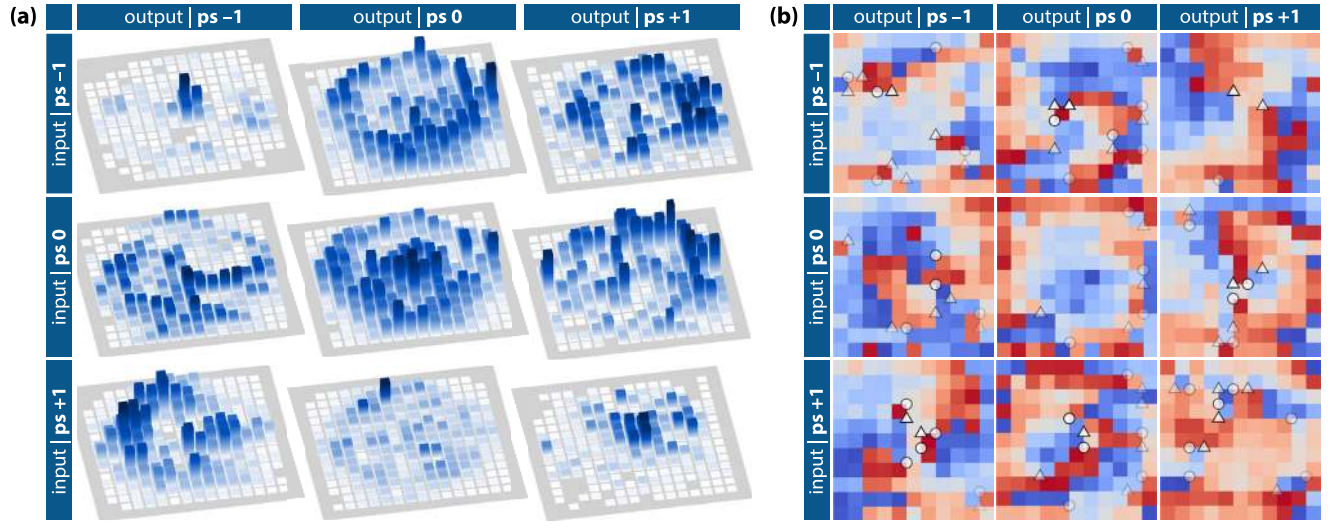

FIG. 5. Experimental observation pseudospin-mediated optical vortex generation. (a) Intensity and (b) phase distribution of the different output pseudospin components as a function of the input eigenstate. White circles (triangles) mark positions of negative (positive) vortices. The opacity of the markers weights the significance of the found vortex (radial gradient). The total vortex charge $l = m_{s,f} - m_{s,i}$ conserves $J_z = L_z + S_z$. Experimental noise and the finite lattice size lead to additional vortex-antivortex pairs.

expanding more slowly, and conversion between different pseudospin eigenstates generating double charge optical vortices. Given other recent advances in designing lattices with arbitrary pseudospin conical intersections [19,20], and realizing them as photonic and optical lattices [15–18], our fundamental concepts and results enable harnessing the unique properties of higher pseudospin states. Possible applications include the controlled generation of nanoscale vortices or vector beams and the conversion of orbital angular momentum between different internal (pseudospin) states.

This work was supported by the Australian Research Council and the German Academic Exchange Service.

*falko.diebel@uni-muenster.de

[1] K. S. Novoselov, A. K. Geim, S. V. Morozov, D. Jiang, M. I. Katsnelson, I. V. Grigorieva, S. V. Dubonos, and A. A. Firsov, Nature (London) **438**, 197 (2005).
[2] M. I. Katsnelson, K. S. Novoselov, and a. K. Geim, Nat. Phys. **2**, 620 (2006).
[3] O. Bahat-Treidel, O. Peleg, M. Grobman, N. Shapira, M. Segev, and T. Pereg-Barnea, Phys. Rev. Lett. **104**, 063901 (2010).
[4] M. Mecklenburg and B. C. Regan, Phys. Rev. Lett. **106**, 116803 (2011).
[5] M. Berry and M. Jeffrey, in *Progress in Optics*, edited by E. Wolf (Elsevier, New York, 2007), Vol. 50, pp. 13–50.
[6] D. Song, V. Paltoglou, S. Liu, Y. Zhu, D. Gallardo, L. Tang, J. Xu, M. Ablowitz, N. K. Efremidis, and Z. Chen, Nat. Commun. **6**, 6272 (2015).
[7] O. Peleg, G. Bartal, B. Freedman, O. Manela, M. Segev, and D. N. Christodoulides, Phys. Rev. Lett. **98**, 103901 (2007).
[8] X. Huang, Y. Lai, Z. H. Hang, H. Zheng, and C. T. Chan, Nat. Mater. **10**, 582 (2011).
[9] M. Bellec, U. Kuhl, G. Montambaux, and F. Mortessagne, Phys. Rev. Lett. **110**, 033902 (2013).
[10] M. Polini, F. Guinea, M. Lewenstein, H. C. Manoharan, and V. Pellegrini, Nat. Nanotechnol. **8**, 625 (2013).
[11] V. Apaja, M. Hyrkäs, and M. Manninen, Phys. Rev. A **82**, 041402 (2010).
[12] R. Shen, L. B. Shao, B. Wang, and D. Y. Xing, Phys. Rev. B **81**, 041410 (2010).
[13] C. Weeks and M. Franz, Phys. Rev. B **82**, 085310 (2010).
[14] N. Goldman, D. F. Urban, and D. Bercioux, Phys. Rev. A **83**, 063601 (2011).
[15] D. Guzmán-Silva, C. Mejía-Cortés, M. A. Bandres, M. C. Rechtsman, S. Weimann, S. Nolte, M. Segev, A. Szameit, and R. A. Vicencio, New J. Phys. **16**, 063061 (2014).
[16] R. A. Vicencio, C. Cantillano, L. Morales-Inostroza, B. Real, C. Mejía-Cortés, S. Weimann, A. Szameit, and M. I. Molina, Phys. Rev. Lett. **114**, 245503 (2015).
[17] S. Mukherjee, A. Spracklen, D. Choudhury, N. Goldman, P. Öhberg, E. Andersson, and R. R. Thomson, Phys. Rev. Lett. **114**, 245504 (2015).
[18] S. Taie, H. Ozawa, T. Ichinose, T. Nishio, S. Nakajima, and Y. Takahashi, Sci. Adv. **1**, e1500854 (2015).
[19] B. Dóra, J. Kailasvuori, and R. Moessner, Phys. Rev. B **84**, 195422 (2011).
[20] Z. Lan, N. Goldman, A. Bermudez, W. Lu, and P. Öhberg, Phys. Rev. B **84**, 165115 (2011).
[21] D. Leykam, O. Bahat-Treidel, and A. S. Desyatnikov, Phys. Rev. A **86**, 031805(R) (2012).
[22] J. D. Malcolm and E. J. Nicol, Phys. Rev. B **90**, 035405 (2014).
[23] M. C. Rechtsman, J. M. Zeuner, Y. Plotnik, Y. Lumer, D. Podolsky, F. Dreisow, S. Nolte, M. Segev, and A. Szameit, Nature (London) **496**, 196 (2013).
[24] M. A. Bandres, M. Rechtsman, A. Szameit, and M. Segev, Lieb Photonic Topological Insulator, in *CLEO: 2014, OSA Technical Digest* (Optical Society of America, 2014) p. FF2D.3.
[25] T. Ando, T. Nakanishi, and R. Saito, J. Phys. Soc. Jpn. **67**, 2857 (1998).
[26] R. A. Sepkhanov, A. Ossipov, and C. W. J. Beenakker, Europhys. Lett. **85**, 14005 (2009).
[27] K. Asano and C. Hotta, Phys. Rev. B **83**, 245125 (2011).
[28] Y. Iye, Proc. Natl. Acad. Sci. U.S.A. **96**, 8821 (1999).
[29] A. Szameit and S. Nolte, J. Phys. B **43**, 163001 (2010).
[30] See Supplemental Material at http://link.aps.org/supplemental/10.1103/PhysRevLett.116.183902 for further discussion of the theoretical modelling and pseudospin filtering.
[31] L. Marrucci, C. Manzo, and D. Paparo, Phys. Rev. Lett. **96**, 163905 (2006).